High-Velocity Compaction of Aluminum Powder by Gas Detonation Forming Technique

Tohid Mirzababaie Mostofi
Faculty of Mechanical Engineering,
University of Eyvanekey, Iran
E-mail: t.m.mostofi@eyc.ac.ir

Mostafa Sayah Badkhor
Faculty of Mechanical Engineering,
University of Eyvanekey, Iran
E-mail: mostafasayah@gmail.com

Hashem Babaei*
Faculty of Mechanical Engineering,
University of Guilan, Iran
E-mail: ghbabaei@guilan.ac.ir
*Corresponding author

Abstract: In this paper, a large-scale experimental study has been conducted in order to evaluate the high-velocity compaction of aluminum powder using Gas Detonation Forming (GDF) processing technique. In this series of experiments, the effect of the distribution of grain particle size, initial powder mass, and loading conditions on green density and strength of compacted products were thoroughly studied. The maximum relative green density and green strength of 97.6% and 17.9% were achieved. Group Method of Data Handling (GMDH)-type neural network in conjunction with Singular Value Decomposition (SVD) method was exerted to model the high-velocity compaction process of aluminum powder. The main objective of this idea is to demonstrate how two characteristics of the high-velocity compaction, namely, the relative green density and strength of products vary with the changing of significant parameters, involved in GDF processing technique.

Biographical notes: Tohid Mirzababaie Mostofi received his PhD in Mechanical Engineering from the University of Guilan, in 2018. He is currently Lecturer at the Department of Mechanical Engineering, University of Eyvanekey, Semnan, Iran. His current research interest includes Impact Mechanics. **Mostafa Sayah Badkhor** received his MSc in Mechanical Engineering from the Ferdowsi University of Mashhad in 2015. **Hashem Babaei** is Assistant Professor of Mechanical engineering at the University of Guilan, Rasht, Iran. He received his PhD in Mechanical Engineering from the University of Guilan. His current research focuses on Impact Mechanics, High-Velocity Forming and Structural Engineering.

1   INTRODUCTION

There has been a progressive demand in powder metallurgy methods because of their broad applications in various fields such as aircraft and automotive industry, production of electronic components, gas turbine technology and manufacturing of cutting tools. This is due to outstanding features of these methods including high material utilization, near net shape tolerances, high production speed along with economic efficiency at high-volume production and the ability to control physical properties such as porosity and density during the compaction process. In conventional powder metallurgy methods, powder particles are blended and placed in the die, then compacted using static or quasi-static hydraulic loads. The compaction loads cause mechanical locking between particles and convert them to a solid state called the green part. At this stage, the mechanical strength of the obtained green parts is not sufficient for industrial applications. Therefore, green parts are ejected from the die, transferred to the furnace and heated up to 80-90 percentage of base metal melting temperature. This causes inter-particle bonding during an atomic diffusion phenomenon called sintering [1-2].

On reviewing the literature [3-10], it appears that the compaction of the metallic powder using both dynamic and static process has been extensively investigated from the viewpoint of the production of nearly fully dense metallic compacts with unique microstructures. In these studies, the influences of temperature and pressure histories, along with the existence of sintering aids, on the final mechanical properties of the resulting metallic compacted product were investigated. However, less experimental and numerical work has been carried out to assess the dynamic compaction of aluminum powders in a quantitative manner, and the physical processes involved in increasing green density, as well as rupture stress, have been poorly comprehended [11-12]. Besides, a good understanding of the influences of loading rate, grain particle size and initial powder mass on mechanical properties of the compact is lacking. It is noteworthy to mention that the behavior of metallic powders subjected to dynamic loads is important for comprehending the performance of metallic armor, as well as the behavior of geological materials for penetration, seismic coupling, and planetary science applications. Several useful references on dynamic compaction can be found in the books by Nesterenko [13] as well as two review papers [14-15]. As mentioned in the literature, important experimental problems that result in rather large scatter and experimental uncertainty is a general specification of investigations of highly distended materials.

In the last decade, the requirement to improve compact properties and to increase manufacturing rates of the compacted product has led to an interest in high-velocity compaction methods. Gas detonation forming (GDF) method is a new technique for forming process, especially powder compaction. This technique differs from the more conventional consolidation methods because of increasing green density, improving green strength, and reducing compact ejection forces as well as the porosity of compacted products. GDF technique can be also used instead of explosive compaction methods because of outstanding features such as low cost, low danger risk, simplicity and the ability to automate the process and continuous production. Recently in a series of studies, Babaei and his colleagues studied empirical and analytical modeling of circular and rectangular plates subjected to various impulsive loading conditions using GDF method [16-21]. They used a mixture of Acetylene and Oxygen gas with different volume ratios and investigated the effects of mechanical properties and geometry of plates, the impulse of applied loads and strain-rate sensitivity on the plastic deformation of plates.

In this paper, the primary objective is to introduce a novel technique, namely, gas mixture detonation method for dynamic compaction process of aluminum powders. An extensive experimental work has been carried out to investigate the influences of different parameters such as grain particle size distribution, initial powder mass, and pre-detonation pressure of Oxygen and Acetylene gas on green density, green strength, porosity, and microstructure of compacted products. Also, an attempt is made to model the powder compaction process using the Group Method of Data Handling (GMDH) algorithm. For constructing numerical models, new dimensionless numbers are suggested based on the effective parameters in gas detonation compaction process.

2   EXPERIMENTAL PROCEDURE

Aluminum powder was used in the current experimental study due to its extensive application potential and high compressibility. The powder was fractioned in three different particle size distributions of 0-50 μm, 50-100 μm, and 100-150 μm. During the compaction process, the initial powder masses were 15 g, 20 g, 25 g, and 30 g. It is noteworthy to mention that the theoretical density ρ_t was 2780 kg·m^{-3}.

Figure 1 shows the photograph of the gas detonation compaction apparatus. As shown in this figure, the apparatus consisted of two main parts, a detonation driver section and the test section. The driver section included of a strong cylindrical combustion chamber with 530 mm length, 210 mm outside diameter, and 120 mm inner diameter, two control valves for filling the chamber with pressurized gas, a manometer gauge to

calculate the pre-detonation pressures of gas, and an ignition system. Detonation pressure-time histories were recorded by a piezoelectric pressure sensor, an amplifier, and a dynamic data acquisition system which were located in the detonation driver unit of the apparatus [12], [16-21].
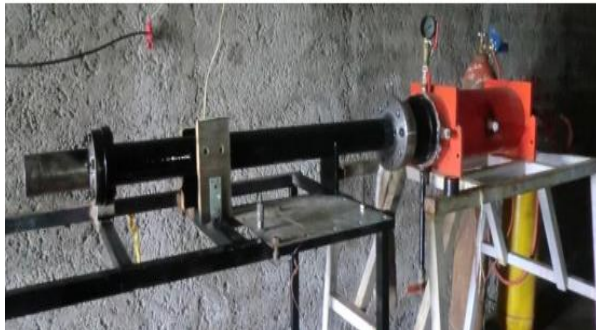
Fig. 1 The gas detonation compaction apparatus.

The test section included of a conical nozzle, an aluminum diaphragm, a barrel with 1040 mm length, 84 mm outside diameter, and 54 mm inner diameter, a 1350 g rigid projectile, a piston, and a floating die with a central hole, which showed the diameter of the compacted product. It is noteworthy to mention that the detonation section was connected to the test section by the conical nozzle [12].

The detonation mixture was a rich mixture of Oxygen and Acetylene gas. By filling the combustion chamber space with the gaseous mixture as well as filling the cylindrical die with unlubricated powder, the compaction process was simply carried out. Before ignition, the piston was brought into contact with tapped powder in the cylindrical die. The gaseous mixture was ignited by the detonation of combustible gas in the combustion chamber and then, detonation wave started moving towards the end of the chamber and arrived at the thin aluminum diaphragm. Next, the detonation wave immediately broke the diaphragm after the first pressure was built up behind the extending detonation. The energy of detonation wave was transmitted to the projectile, hence, it moved towards the end of the barrel and impacted onto the piston. As a result, this was pursued by applying an axial load, which led to compress the powder from one side. Eventually, the floating die was removed at the end of the compaction process and a hydraulic jack was used for ejecting the cylindrical compacted product from the die.

The diametral compression test which is called the Brazilian disc test was considered to be an accurate and reliable approach to determine the green strength of compacted products. During the Brazilian disc test, a thin disc was compressed across a diameter to failure. The material strength was calculated based on the assumption that failure begins at the point of maximum stress. To perform the compression tests, all specimens were mounted on a universal testing machine with a crosshead speed of 0.5 mm/min and were located between two flat plates.

In order to calculate the green strength of compacted products from the Brazilian disc test, "Eq. (1)" was used in which the maximum load value at failure was substituted in this equation [22].

$$\sigma_g = \frac{2F}{\pi D H_f} \tag{1}$$

Where, F is maximum load at failure, H_f and D are height and diameter of the compacted product.

3   EXPERIMENTAL RESULTS

"Table 1" summarizes the experimental results from the gas detonation compaction experiments. As presented in "Table 1", all one-sided compacted specimens were obtained from a 21 mm cylindrical die and were manufactured in groups of densities ranging from 2493.3 kg·m^{-3} to 2714.4 kg·m^{-3}.

Table 1 Experimental results

Test No	P_{total}, bar	H_0, mm	ρ_g, kg·m^{-3}	σ_g, MPa
1	2	38.8	2714.4	21.46
2	1.5	38.8	2668.2	19.08
3	1	38.8	2619.6	16.17
4	0.5	38.8	2532.6	12.53
5	2	48.8	2703	20.75
6	1.5	48.8	2650.5	18.33
7	1	48.8	2610.7	14.53
8	0.5	48.8	2525.1	11.75
9	2	58.8	2699.1	20.02
10	1.5	58.8	2644.6	16.07
11	1	58.8	2594	12.22
12	0.5	58.8	2514.8	8.89
13	2	68.8	2688.8	17.40
14	1.5	68.8	2637.4	13.75
15	1	68.8	2588.7	11.24
16	0.5	68.8	2501.2	7.45
17	2	38.8	2711.3	19.97
18	1.5	38.8	2665.2	16.38
19	1	38.8	2616.3	13.43
20	0.5	38.8	2531.7	9.58
21	2	48.8	2700.5	19.48
22	1.5	48.8	2649.1	15.81
23	1	48.8	2606.5	12.49

24	0.5	48.8	2522.9	8.74
25	2	58.8	2690.8	17.81
26	1.5	58.8	2639.3	13.61
27	1	58.8	2591.5	10.42
28	0.5	58.8	2508.7	6.72
29	2	68.8	2680.2	15.77
30	1.5	68.8	2631.8	12.45
31	1	68.8	2582.6	9.40
32	0.5	68.8	2494.8	4.79
33	2	38.8	2709.4	18.32
34	1.5	38.8	2657.4	15.08
35	1	38.8	2611.8	11.11
36	0.5	38.8	2529.2	7.37
37	2	48.8	2701	16.98
38	1.5	48.8	2646.8	14.35
39	1	48.8	2604	10.56
40	0.5	48.8	2521.7	6.65
41	2	58.8	2687.4	15.53
42	1.5	58.8	2633.5	12.51
43	1	58.8	2586.5	8.95
44	0.5	58.8	2509.2	4.88
45	2	68.8	2678	14.38
46	1.5	68.8	2619.9	11.43
47	1	68.8	2579.3	8.43
48	0.5	68.8	2493.4	3.42

Several aluminum powder compacts produced by gas mixture detonation method have been shown in Fig. 2.

Fig. 2   Aluminum powder compacts.

For a better understanding of the obtained results, the experimental curves of the percentage relative green density versus total pre-detonation pressure of gaseous mixture have been represented in "Fig. 3", for the cases, when the value of grain particle size is constant in each figure and the amount of initial powder mass is changed. As shown in "Fig. 3", the relative green density of compacted products gradually increased with total pre-detonation pressure rising. It was clear that the figures demonstrated two steps with the different increasing rate of relative green density.
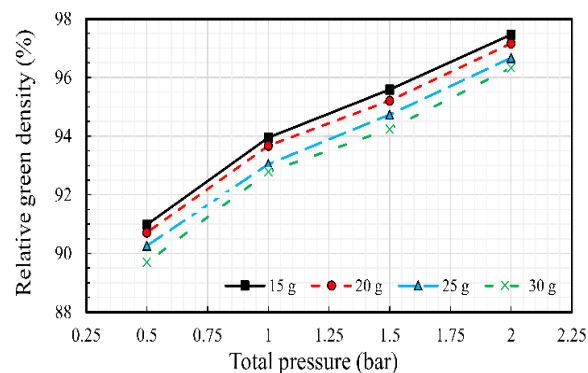
(a) $\lambda = 50 \ \mu m$
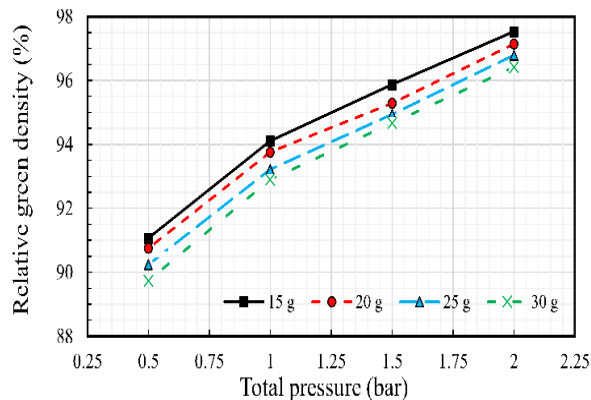
(b) $\lambda = 100 \ \mu m$
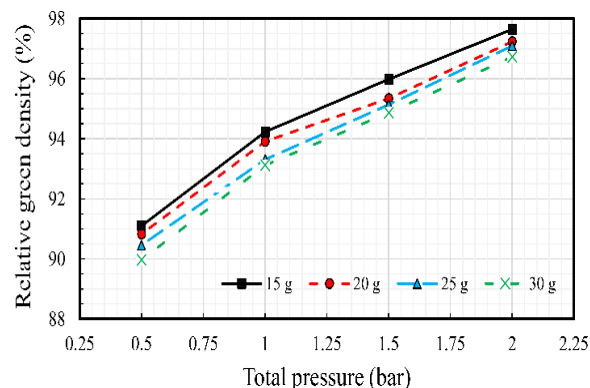
(c) $\lambda = 150 \ \mu m$

Fig. 3   Percentage relative green density versus total pre-detonation pressure.

In the first step, for the case when the total pre-detonation pressure was less than 1 bar, the percentage relative green density considerably increased. For instance, in "Fig. 2a", when the total pre-detonation pressure increased to 1 bar from 0.5 bar, the percentage relative green density of 15 g samples reached 93.95% from 90.98% at a rate of 5.94 bar^{-1}. However, in the next stage, *i.e.* when the total pre-detonation pressure was more than 1 bar, the relative green density slowly increased. On the other word, when the total pre-detonation pressure increased to 2 bar from 1 bar, the

percentage relative green density of 15 g samples reached 97.46% from 93.95% at a rate of 3.51 bar^{-1}. By calculating the rates for all specimens, it was observed that the increasing rate of the first step of densification is approximately 1.69 (6.03/3.56) times larger than that of the second one. This is because of that, in the first step, densification of compacted products mainly happened in the form of particle displacements as well particle rearrangements, consequently, the relative green density increased quickly by increasing total pre-detonation pressure of the gaseous mixture. Although, in the second step, the released energy acting on powder structure was dissipated for sliding, rotating, deforming and breaking the particles. As a result, the increasing rate of relative green density at the second step was lower than the first one.

In order to investigate the effect of grain particle size on the amount of percentage relative green density, the experimental curve of percentage relative green density versus total pre-detonation pressure has been shown in "Fig. 4".
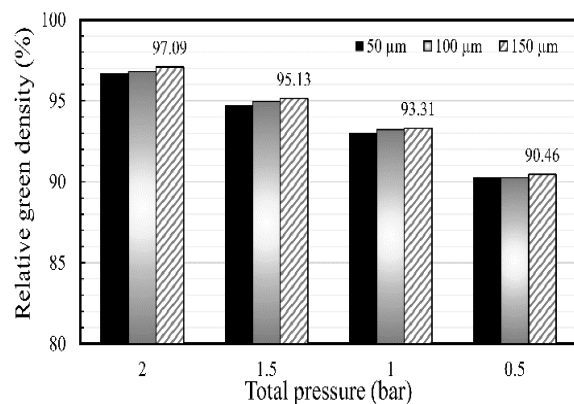
Fig. 4   Percentage relative green density versus total pre-detonation pressure (M₀ = 25 g).

This figure was presented only for 25 g samples because the other specimens had the same behavior. A closer look at "Fig. 4" represented that the percentage relative green densities of compacted products did not increase significantly with grain particle size rising. Hence, it can be concluded that the increase of grain particle size does not have much effect on the increase of green density of compacted products.

The experimental curves of green strength versus total pre-detonation pressure of gaseous mixture have been represented in "Fig. 5" for the cases when the value of grain particle size is constant in each figure and the amount of initial powder mass is changed. As represented in "Fig. 5", the green strength of compacted products gradually increased by an increase in total pre-detonation pressure. Moreover, as total pre-detonation pressure increases, the kinetic energy is increased obviously.

(a) $\lambda = 50 \ \mu m$

(b) $\lambda = 100 \ \mu m$

(c) $\lambda = 150 \ \mu m$
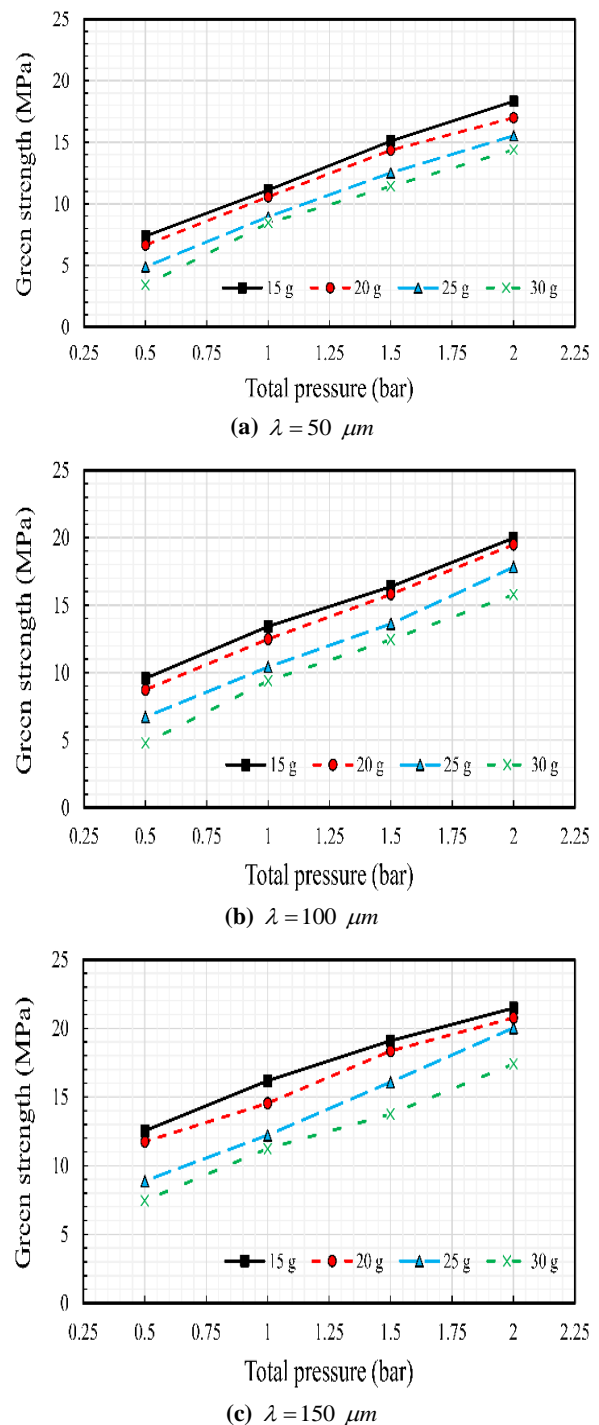
Fig. 5   Percentage relative green strength versus total pre-detonation pressure.

Hence, the kinetic energy applying on powder particles will increase and this will cause deformation and displacement of the particles more easily. Consequently, the bonding will be improved significantly for the mechanical interlocking between the powder particles as well as the cold welding.

In order to investigate the effect of grain particle size on the amount of green strength, the experimental curve of green strength versus total pre-detonation pressure has been shown in "Fig. 6".
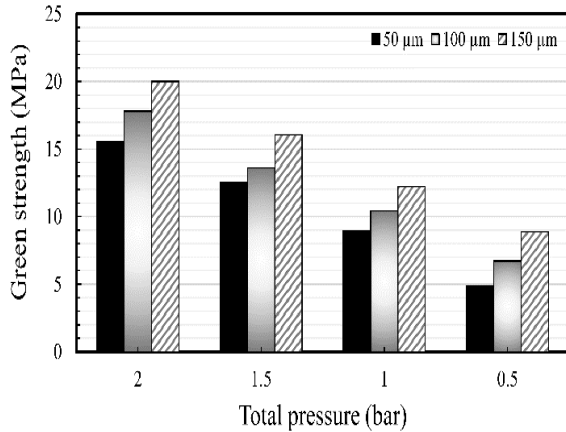
Fig. 6   Green strength versus total pre-detonation pressure (M_0 = 25 g).

This figure was presented only for 25 g samples because the other specimens had the same behavior. A closer look at "Fig. 5" represented that the green strengths of compacted products increased significantly with grain particle size rising. Hence, it can be concluded that unlike green density, the increase of grain particle size has a considerable effect on the increase of green density of compacted products.

4   MODELLING USING GMDH-TYPE NEURAL NETWORKS

The classical GMDH algorithm can be represented as a set of neurons in which different pairs of them in each layer are connected through a quadratic polynomial and thus produce new neurons in the next layer. Such representation can be used in modelling to map inputs to outputs. The formal definition of the identification problem is to find a function $\hat{f}$ which can be approximately used instead of actual one, f, in order to predict output $\hat{y}$ for a given input vector $X = (x_1, x_2, x_3, \ldots, x_n)$ as close as possible to its actual output y. Therefore, given M observation of multi-input-single-output data pairs so that [11].

$$y_i = f(x_{i1}, x_{i2}, x_{i3}, \ldots, x_{in}) \ (i = 1, 2, 3, \ldots, M) \qquad (2)$$

It is now possible to train a GMDH-type neural network to predict the output values $\hat{y}_i$ for any given input vector $X_i = (x_{i1}, x_{i2}, x_{i3}, \ldots, x_{in})$, that is:

$$\hat{y}_i = \hat{f}(x_{i1}, x_{i2}, x_{i3}, \ldots, x_{in}) \ (i = 1, 2, 3, \ldots, M) \qquad (3)$$

The problem is now to determine a GMDH-type neural network so that the square of the difference between the actual output and the predicted one is minimized, that is:

$$\sum_{i=1}^{M} \left[\hat{f}(x_{i1}, x_{i2}, x_{i3}, \ldots, x_{in}) - y_i \right]^2 \to \min \qquad (4)$$

The general connection between inputs and output variables can be expressed by a complicated polynomial of the form:

$$y = a_0 + \sum_{i=1}^{n} a_i x_i + \sum_{i=1}^{n}\sum_{j=1}^{n} a_{ij} x_i x_j + \sum_{i=1}^{n}\sum_{j=1}^{n}\sum_{k=1}^{n} a_{ijk} x_i x_j x_k$$

$$(5)$$

Which is known as the Ivakhnenko polynomial [11]. However, for most application, the quadratic form of only two variables is used in the form:

$$\hat{y} = G(x_i, x_j) = a_0 + a_1 x_i + a_2 x_j + a_3 x_i x_j + a_4 x_i^2 + a_5 x_j^2$$

$$(6)$$

To predict the output y, The coefficient a_i in "Eq. (6)" are calculated using regression techniques, so that the difference between actual output, y and the calculated one, $\hat{y}$, for each pair of x_i, x_j as input variables are minimized. Indeed, it can be seen that a tree of polynomials is constructed using the quadratic form given in "Eq. (6)" whose coefficients are obtained in a least-squares sense. In this way, the coefficients of each quadratic function G_i are obtained to optimally fit the output in the whole set of input-output data pair, that is:

$$r^2 = \frac{\sum_{i=1}^{M} \left(y_i - G_i(\ ) \right)^2}{\sum_{i=1}^{M} y_i^2} \qquad (7)$$

In the basic form of the GMDH algorithm, all the possibilities of two independent variables out of total n input variables are taken in order to construct the regression polynomial in the form of "Eq. (6)" that best fits the dependent observations ($y_i, i = 1, 2, \ldots, M$) in a least-squares sense. Consequently, $\binom{n}{2} = \dfrac{n(n-1)}{2}$ neurons will be built up in the second layer of the feedforward network from the observations

$$\left\{\left(y_i, x_{ip}, x_{iq}\right); \left(i = 1, 2, ..., M\right)\right\}$$

for different $p, q \in \{1, 2, ..., M\}$. In other words, it is now possible to construct M data triples $\left\{\left(y_i, x_{ip}, x_{iq}\right); \left(i = 1, 2, ..., M\right)\right\}$ from observation using such $p, q \in \{1, 2, ..., M\}$ in the form:
$$\begin{bmatrix} x_{1p} & x_{1q} & y_1 \\ x_{2p} & x_{2q} & y_2 \\ M & M & M \\ x_{Mp} & x_{Mq} & y_M \end{bmatrix}.$$

Using the quadratic sub-expression in the form of "Eq. (6)" for each row of M data triples, the following matrix equation can be readily obtained as:

$$A\mathbf{a} = Y \tag{8}$$

Where $\mathbf{a}$ is the vector of unknown coefficients of the quadratic polynomial in "Eq. (6)".

$$\mathbf{a} = \{a_0, a_1, a_2, a_3, a_4, a_5\} \tag{9}$$

And:

$$Y = \{y_1, y_2, y_3, ..., y_M\}^T \tag{10}$$

Where Y is the vector of output's value from observation. It can be readily seen that:

$$A = \begin{bmatrix} 1 & x_{1p} & x_{1q} & x_{1p}x_{1q} & x_{1p}^2 & x_{1q}^2 \\ 1 & x_{2p} & x_{2q} & x_{2p}x_{2q} & x_{2p}^2 & x_{2q}^2 \\ M & M & M & M & M & M \\ 1 & x_{Mp} & x_{Mq} & x_{Mp}x_{Mq} & x_{Mp}^2 & x_{Mq}^2 \end{bmatrix} \tag{11}$$

The least-squares technique from multiple-regression analysis leads to the solution of the normal equations in the form of:

$$\mathbf{a} = \left(A^T A\right)^{-1} A^T Y \tag{12}$$

Which determines the vector of the best coefficients of the quadratic "Eq. (6)" for the whole set of M data triples. However, such a solution directly from normal equations is rather susceptible to round off error and, more importantly, to the singularity of these equations. SVD is the method for solving most linear least squares problems where some singularities may exist in the normal equations. The SVD of a matrix, $A \in \Re^{M \times 6}$, is a factorization of the matrix into the product of three matrices, column-orthogonal matrix $U \in \Re^{M \times 6}$, diagonal matrix $W \in \Re^{6 \times 6}$ with non-negative elements (singular values), and orthogonal matrix $V \in \Re^{6 \times 6}$ such that:

$$A = UWV^T \tag{13}$$

The most popular technique for computing the SVD was originally proposed in [23-29]. The problem of optimal selection of vector of the coefficients in "Eqs. (9) and (12)" is first reduced to find the modified inversion of diagonal matrix W, in which the reciprocals of zero or near zero singulars (according to a threshold) are set to zero. Then, such optimal $\mathbf{a}$ is calculated using the following relation.

$$\mathbf{a} = V\left[diag\left(\frac{1}{w_j}\right)\right]U^T Y \tag{14}$$

Such procedure of SVD approach of finding the optimal coefficients of quadratic polynomials, $\mathbf{a}$, improves the performance of self-organizing GMDH type algorithms that are employed to build networks based on input-output observation data triples.

5 STRUCTURE IDENTIFICATION OF GMDH-TYPE NETWORKS

For simultaneous determination of structure and parametric identification of GMDH-type neural networks, the numbers of layers, as well as the number of neurons in each layer, is determined according to a threshold for error "Eq. (6)". In addition, unlike two previous approaches, some of the input variables or generated neurons in different layers can be included in subsequent layers. The main steps of this approach are described as follows [11]:

- Step 1: Set K=1, Set Threshold.

- Step 2: Construct $N_k' = N_k\left(N_k - 1\right)/2$ neurons according to all possibilities of connection by each pair of neurons in the layer. This can be achieved by forming the quadratic expression $G\left(x_i, x_j\right)$ which approximates the output y in "Eq. (6)" with least-squares errors of "Eq. (7)" either by solving the normal "Eq. (12)" or by SVD approach "Eq. (14)".

- Step 3: Select the single best neuron out of these N_k' neurons, x', according to its value of r^2. If (Error < Threshold) Then END, Otherwise set

Vec_of_Var$=\{x_1, x_2, x_3, ..., x_n, x'\}$

- Step 4: Set $N_k = N_k + 1$; go to 2.

6 NUMERICAL MODELLING RESULTS

The method described in previous sections is now used to design GMDH-type network systems for a set of dimensionless parameters constructed upon experimental input-output data in a series of compaction tests given in "Table 1". Accordingly, the set of output-inputs variables used to train the GMDH-type neural network is a dimensionless set, $\Pi = \{\pi_1, \pi_2, \pi_3, ..., \pi_k\}$, rather than the set of real physical variables $\{y, X\} = \{y, x_1, x_2, x_3, ..., x_n\}$. Hence, given M observation of multi-input-single-output data pairs which have been converted to the equivalent dimensionless parameter [11-12], [24].
So that:

$$\pi_{1i} = f\left(\pi_{2i}, \pi_{3i}, \pi_{4i}, ..., \pi_{ki}\right)\left(i = 1, 2, 3, ..., M\right) \quad (15)$$

It is now possible to train a GMDH-type neural network to predict the output values $\hat{\pi}_{1i}$ for any given input vector $\left(\pi_{2i}, \pi_{3i}, \pi_{4i}, ..., \pi_{ki}\right)$, that is:

$$\hat{\pi}_{1i} = \hat{f}\left(\pi_{2i}, \pi_{3i}, \pi_{4i}, ..., \pi_{ki}\right)\left(i = 1, 2, 3, ..., k\right) \quad (16)$$

The problem is now to determine a GMDH-type neural network so that the square of the difference between the actual dimensionless output and the predicted one is minimized, that is:

$$\sum_{i=1}^{M}\left[\hat{f}\left(\pi_{2i}, \pi_{3i}, \pi_{4i}, ..., \pi_{ki}\right) - \hat{\pi}_{1i}\right]^2 \to \min \quad (17)$$

Again, the quadratic form of only two variables is used in the form of "Eq. (18)" to predict the output π_1.

$$\hat{\pi}_1 = G\left(\pi_i, \pi_j\right) = a_0 + a_1\pi_i + a_2\pi_j + a_3\pi_i\pi_j$$
$$+ a_4\pi_i^2 + a_5\pi_j^2 \quad (18)$$

In high-velocity powder compaction process using gas detonation forming method, the percentage relative green density ($\rho_{rel} = \rho_g / \rho_t \times 100$) and the percentage relative green strength ($\sigma_{rel} = \sigma_g / \sigma_t \times 100$) of compacted products can be expressed based on effective

parameters including the pre-detonation pressure of Oxygen (P_{O_2}) and Acetylene ($P_{C_2H_2}$) in the chamber, the initial powder mass (M_0) and height of powder in the die (H_0), the density of powder in the die before compaction (ρ_0), the final powder mass (M_f) and height of compacted products (H_f), the diameter of the die (D), the sound velocity in Oxygen ($C_{O_2} = 332.2\,m/s$) and Acetylene ($C_{C_2H_2} = 329\,m/s$) and the grain particles size (λ). These parameters have been considered to generate 5 dimensionless numbers in a neural network. From this set of input-output parameters, 5 independent dimensionless numbers have been constructed according to 3 main dimensions (M, L, T), as follows:

$$\pi_1 = \rho_{rel} \quad (19)$$

$$\pi_1' = \sigma_{rel} \quad (20)$$

$$\pi_2 = \frac{\rho_0 C_{O_2} C_{H_2O_2}}{P_{O_2} + P_{C_2H_2}} \quad (21)$$

$$\pi_3 = \frac{M_f}{M_0} \quad (22)$$

$$\pi_4 = \frac{\lambda}{D} \quad (23)$$

$$\pi_5 = \frac{H_f}{H_0} \quad (24)$$

So that:

$$\pi_1, \pi_1' = f\left(\pi_2, \pi_3, \pi_4, \pi_5\right) \quad (25)$$

It should be noted that the simplest possible dimensionless parameters have been considered according to the involved physical parameters.
In order to model, based on experimental data presented in "Table 1", the multi-input-single-output set of constructed dimensionless data according to "Eqs. (19)-(24)", the method previously mentioned was used separately in conjunction with the SVD approach for the coefficient of the quadratic polynomials. In order to demonstrate the prediction ability of such GMDH-type neural networks in the case of dimensionless modelling, the data have been randomly divided into two different sets, namely, training and testing sets. The training set,

which consists of 32 out of 48 input-output data pairs, is used for training the GMDH-type neural network models using SVD approach for the coefficients of the quadratic polynomials. The predicting set, which consists of 16 unforeseen inputs-output data samples during the training process, is merely used for predicting to show the prediction ability of such GMDH-type neural networks models during the training process.
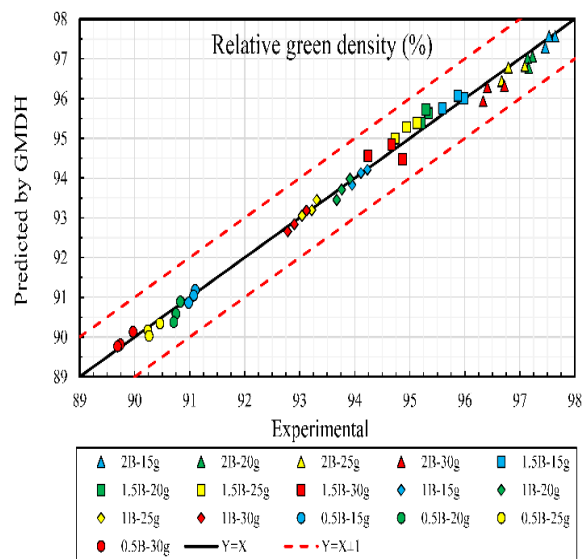
Fig. 7   Comparison of experimental results with computed/predicted values by GMDH-type network.
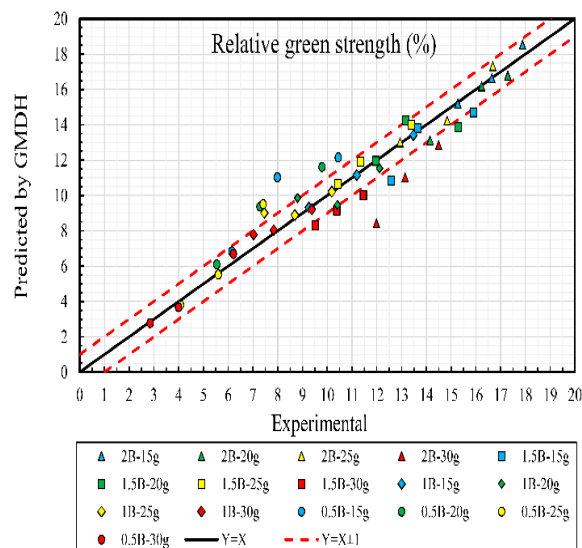
Fig. 8   Comparison of experimental results with computed/predicted values by GMDH-type network.

Accordingly, "Figs. 7-8" show the relative green density and strength of aluminum powder compacts, respectively, using GMDH-type network model constructed with singular value decomposition approach

for the coefficients of the quadratic polynomials. The solid line in the following figures is where the experimental and numerical values of (ρ_{rel}) and (σ_{rel}) are equal. Also, the red dash lines in these figures are "Eq. (A.22) $\pm (\rho_{rel})$ and Eq. (A.50) $\pm (\sigma_{rel})$" which have been drawn for the aim of displaying the fitting accuracy.

The results of "Fig. 7" show that all experimental data points in "Table 1" fall inside the 90% confidence level and the presented polynomial equations based on the structure of the GMDH-type neural network can be successfully used for prediction of the percentage relative green density compacted products by gas detonation forming method. Also, the results of "Fig. 8" demonstrate that the present experimental data points fall into the $\pm(\sigma_{rel})$ range from the solid line with a confidence level of 73%. The structures of GMDH-type network for prediction of the relative green density and strength of products have been depicted in "Figs 9-10", respectively.
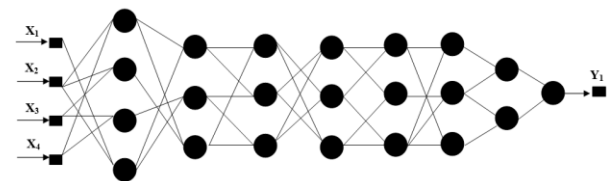
Fig. 9   GMDH-type network for prediction of the relative green density.
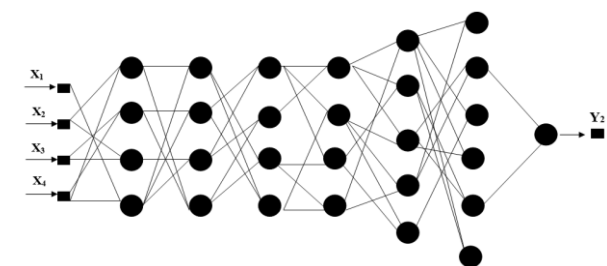
Fig. 10   GMDH-type network for prediction of the relative green strength.

By considering aforementioned points, the application and validity of suggested dimensionless numbers and GMDH-type network were proved and it is concluded that these suggested numbers can be used successfully for determination and predicting the final mechanical properties of compacted products by gas detonation forming method. The best point is that the suggested dimensionless numbers, as well as polynomial equations, considered many effective parameters of the processing technique. However, more experimental studies on metallic powder with different grain particle size distributions and mechanical properties should be carried out to develop the network.

7   CONCLUSION

In this paper, a novel processing technique, namely, gas detonation forming method was introduced and used for powder compaction. According to this new idea, high-velocity compaction of aluminum powder was investigated experimentally. On returning to the literature review, the obtained results were the first quantitative experiments on compaction of aluminum powder by gas detonation forming method.

In the experimental section, 48 experiments were carried out by gas mixture detonation apparatus at four different total pre-detonation pressure of the gaseous mixture, three different grain particle size distribution and also, three different initial powder masses. The detonation loads were generated by a detonating mixture of Acetylene and Oxygen gas in a combustion chamber, while the detonation pressure was measured by means of a piezoelectric sensor and dynamic data acquisition system. The energy of detonation wave was transmitted to the projectile, hence it moved towards the end of the barrel and impacted onto the piston. As a result, this was pursued by applying an axial load, which led to compress the powder from one side. The main experimental results are:

• The relative green density of products gradually increased with total pre-detonation pressure rising and the increasing rate of the first step of densification is approximately 1.69 times larger than that of the second one.

• The green strength of products gradually increased by the increase of pre-detonation pressure.

• Unlike green density, the increase of grain particle size has a considerable effect on the increase of green density of the product.

GMDH-type networks were successfully used for the modelling of the very complex process of high-velocity compaction of aluminum powder. In this way, it has been shown that GMDH-type networks provide effective means to model and predict the relative green density and strength of products by GDF processing technique according to different inputs. Moreover, it has been shown that SVD can significantly improve the performance of such GMDH-type networks.

8   APPENDIX OR NOMENCLATURE

The obtained polynomial equations for the percentage relative green density compacted products based on the structure of the GMDH-type neural network depicted in "Fig. 9" using SVD approach for the coefficient of the quadratic polynomials in the form of:

$$Z_1 = 343.9 - 371.8X_2 - 347.7X_4 - 27.29X_2{}^2 \\ - 759.1X_4{}^2 + 1022X_2X_4 \tag{A.1}$$

$$Z_2 = 529.2 - 860.1X_2 - 8890X_3 + 425.7X_2{}^2 \\ + 164900X_3{}^2 + 7481X_2X_3 \tag{A.2}$$

$$Z_3 = 140.2 - 503.1X_3 - 164.2X_4 + 44830X_3{}^2 \\ + 137.7X_4{}^2 - 356.5X_3X_4 \tag{A.3}$$

$$Z_4 = 0.0005309 + 0.2147X_1 + 0.0002843X_2 \\ - 0.00003890X_1{}^2 + 0.00007620X_2{}^2 - 0.08479X_1X_2 \tag{A.4}$$

$$W_1 = -0.004838 - 0.2441Z_1 + 1.543Z_4 + 0.01472Z_1{}^2 \\ + 0.001134Z_4{}^2 - 0.01907Z_1Z_4 \tag{A.5}$$

$$W_2 = -0.01367 - 0.7099Z_3 + 2.005Z_4 + 0.01892Z_3{}^2 \\ + 0.0004633Z_4{}^2 - 0.02256Z_3Z_4 \tag{A.6}$$

$$W_3 = 0.009699 + 0.4573Z_1 + 0.4576Z_2 - 0.09201Z_1{}^2 \\ - 0.09220Z_2{}^2 + 0.1851Z_1Z_2 \tag{A.7}$$

$$U_1 = 0.01004 + 0.4806W_1 + 0.4746W_3 - 0.1170W_1{}^2 \\ - 0.1199W_3{}^2 + 0.2373W_1W_3 \tag{A.8}$$

$$U_2 = 0.01061 + 0.5031W_1 + 0.5032W_2 + 0.1013W_1{}^2 \\ + 0.09834W_2{}^2 - 0.1997W_1W_2 \tag{A.9}$$

$$U_3 = 0.009131 + 0.4360W_2 + 0.4320W_3 - 0.1275W_2{}^2 \\ - 0.1277W_3{}^2 + 0.2566W_2W_3 \tag{A.10}$$

$$S_1 = -0.009736 + 0.4939U_2 + 0.5329U_3 + 1.555U_2{}^2 \\ + 1.555U_3{}^2 - 3.110U_2U_3 \tag{A.11}$$

$$S_2 = 0.009821 + 0.4827U_1 + 0.5526U_3 + 0.9518U_1{}^2 \\ + 0.9523U_3{}^2 - 1.905U_1U_3 \tag{A.12}$$

$$S_3 = 0.01169 + 0.4745U_1 + 0.5112U_2 - 0.4568U_1^2 \\ -0.4563U_2^2 - 0.9133U_1U_2$$

(A.13)

$$R_1 = -0.008061 + 0.5967S_1 + 0.3577S_2 - 1.701S_1^2 \\ -1.710S_2^2 + 3.411S_1S_2$$

(A.14)

$$R_2 = 0.01028 + 0.5075S_1 + 0.4963S_3 + 0.3629S_1^2 \\ +0.3606S_3^2 - 0.7236S_1S_3$$

(A.15)

$$R_3 = 0.01281 + 0.5136S_2 + 0.4913S_3 + 0.2988S_2^2 \\ +0.2961S_3^2 - 0.5949S_2S_3$$

(A.16)

$$H_1 = 0.01501 + 0.9345R_1 + 0.1250R_3 + 2.688R_1^2 \\ +2.684R_3^2 - 5.372R_1R_3$$

(A.17)

$$H_2 = -0.02733 + 0.4575R_2 + 0.4874R_3 - 3.527R_2^2 \\ -3.542R_3^2 + 7.070R_2R_3$$

(A.18)

$$H_3 = -0.03653 + 0.1598R_1 + 0.7789R_2 - 2.598R_1^2 \\ -2.599R_2^2 + 5.198R_1R_2$$

(A.19)

$$T_1 = 0.001090 + 0.4838H_1 + 0.4339H_2 - 1.229H_1^2 \\ -1.238H_2^2 + 2.467H_1H_2$$

(A.20)

$$T_2 = 0.0007697 + 0.4693H_2 + 0.4880H_3 - 1.064H_2^2 \\ -1.060H_3^2 + 2.124H_2H_3$$

(A.21)

$$Y_1 = 0.005745 + 0.4836T_1 + 0.5193T_2 + 0.2813T_1^2 \\ +0.2770T_2^2 - 0.5583T_1T_2$$

(A.22)

$$Z_1' = 295.6 - 351.9X_2 - 489.2X_4 - 67.59X_2^2 \\ -698.1X_4^2 + 1097X_2X_4$$

(A.23)

$$Z_2' = 78.74 - 30.15X_3 - 244.1X_4 + 100400X_3^2 \\ +198.7X_4^2 - 1762X_3X_4$$

(A.24)

$$Z_3' = 472.7 - 888.7X_2 - 8807X_3 + 425.4X_2^2 \\ +251500X_3^2 + 6736X_2X_3$$

(A.25)

$$Z_4' = 0.0001730 + 0.06232X_1 + 0.0000829X_2 \\ -0.00000571X_1^2 + 0.00000704X_2^2 - 0.04845X_1X_2$$

(A.26)

$$W_1' = 2.384 - 0.2225Z_1' + 1.002Z_4' + 0.03348Z_1'^2 \\ -0.05771Z_4'^2 + 0.02644Z_1'Z_4'$$

(A.27)

$$W_2' = 4.999 - 0.7225Z_2' + 0.9766Z_4' + 0.03645Z_2'^2 \\ -0.07370Z_4'^2 + 0.06533Z_2'Z_4'$$

(A.28)

$$W_3' = -5.161 + 0.8018Z_3' + 1.429Z_4' + 0.03288Z_3'^2 \\ -0.03304Z_4'^2 - 0.06501Z_3'Z_4'$$

(A.29)

$$W_4' = -0.06884 + 2.525Z_1' - 1.530Z_2' + 0.2578Z_1'^2 \\ +0.3907Z_2'^2 - 0.6491Z_1'Z_2'$$

(A.30)

$$U_1' = 1.106 + 0.3400W_2' + 0.3473W_3' + 0.07924W_2'^2 \\ +0.08270W_3'^2 - 0.1456W_2'W_3'$$

(A.31)

$$U_2' = 0.5043 + 0.9750W_3' - 0.1659W_4' + 0.04383W_3'^2 \\ +0.08906W_4'^2 - 0.1219W_3'W_4'$$

(A.32)

$$U_3' = -1.679 + 1.829W_1' - 0.6536W_4' + 0.3896W_1'^2 \\ +0.4477W_4'^2 - 0.8421W_1'W_4'$$

(A.33)

$$U_4' = 0.4986 + 0.7215W_1' + 0.1275W_3' + 0.1148W_1'^2 \\ +0.1270W_3'^2 - 0.23391W_1'W_3'$$

(A.34)

$$S_1' = 0.5233 + 3.400U_1' - 2.493U_2' - 0.9808U_1'^2 \\ -0.7588U_2'^2 + 1.745U_1'U_2'$$

(A.35)

$$S_2' = -0.3513 + 2.049U_1' - 0.9704U_4' + 0.01391U_1'^2 \\ +0.07636U_4'^2 - 0.09412U_1'U_4'$$

(A.36)

$$S_3' = -0.1235 + 0.7555U_1' + 0.2807U_3' - 0.1693U_1'^2 \\ -0.1821U_3'^2 + 0.3499U_1'U_3'$$

(A.37)

$$S_4' = -0.4251 + 0.7048U_3' + 0.3423U_4' + 0.5657U_3'^2$$
$$+0.6014U_4'^2 - 1.169U_3'U_4' \tag{A.38}$$

$$R_1' = -0.1135 + 0.1899S_1' + 0.8205S_4' + 0.1575S_1'^2$$
$$+0.09118S_4'^2 - 0.2489S_1'S_4' \tag{A.39}$$

$$R_2' = 0.2025 + 0.4657S_1' + 0.4987S_3' - 0.1543S_1'^2$$
$$-0.1939S_3'^2 + 0.3498S_1'S_3' \tag{A.40}$$

$$R_3' = -0.03952 + 0.7170S_1' + 0.2841S_2' + 0.1616S_1'^2$$
$$+0.1463S_2'^2 - 0.3079S_1'S_2' \tag{A.41}$$

$$R_4' = -0.01423 - 0.4712S_2' + 1.505S_4' - 0.8605S_2'^2$$
$$-0.9581S_4'^2 + 1.817S_2'S_4' \tag{A.42}$$

$$R_5' = 0.6767 - 0.6939S_2' + 1.580S_3' - 2.140S_2'^2$$
$$-2.2981S_3'^2 + 4.444S_2'S_3' \tag{A.43}$$

$$H_1' = 0.3096 + 0.6959R_1' + 0.2454R_4' - 1.021R_1'^2$$
$$-1.036R_4'^2 + 2.060R_1'R_4' \tag{A.44}$$

$$H_2' = 0.4894 + 0.5924R_3' + 0.3318R_4' - 0.8897R_3'^2$$
$$-0.9086R_4'^2 + 1.802R_3'R_4' \tag{A.45}$$

$$H_3' = 0.4278 + 0.8936R_1' + 0.03248R_5' - 0.5559R_1'^2$$
$$-0.5521R_5'^2 + 1.111R_1'R_5' \tag{A.46}$$

$$H_4' = 0.2659 + 1.189R_1' - 0.2200R_3' - 3.694R_1'^2$$
$$-3.705R_3'^2 + 7.400R_1'R_3' \tag{A.47}$$

$$H_5' = -1.507 + 10.18R_2' - 8.951R_3' + 12.94R_2'^2$$
$$+13.54R_3'^2 - 26.49R_2'R_3' \tag{A.48}$$

$$H_6' = -0.06030 - 0.3525R_1' + 1.359R_2' + 0.8930R_1'^2$$
$$+0.8223R_2'^2 - 1.716R_1'R_2' \tag{A.49}$$

$$Y_2 = 0.7150 + 1.022H_2 - 0.1387H_5' - 5.400H_2'^2$$
$$-5.319H_5'^2 + 10.72H_2'H_5' \tag{A.50}$$

REFERENCES

[1] Berg, S., Jonsén, P., and Häggblad, H. A., Experimental Characterisation of CaCO3 Powder Mix for High-Pressure Compaction Modelling, Powder Technol., Vol. 203, No. 2, 2010, pp. 198–205.

[2] Berg, S., Häggblad, H. A., and Jonsén, P., High-Pressure Compaction Modelling of Calcite (CaCO3) Powder Compact, Powder Technol., Vol. 206, No. 3, 2011, pp. 259–268.

[3] Yan, Z., Chen, F., and Cai, Y., High-Velocity Compaction of Titanium Powder and Process Characterization, Powder Technol., Vol. 208, No. 3, 2011, pp. 596–599.

[4] Al-Qureshi, H. A., Galiotto, A., and Klein, A. N., On the Mechanics of Cold die Compaction for Powder Metallurgy, J. Mater. Process, Technol., Vol. 166, No. 1, 2005, pp. 135–143.

[5] Al-Qureshi, H. A., Soares, M. R. F., Hotza, D., Alves, M. C., and Klein, A. N., Analyses of the Fundamental Parameters of Cold Die Compaction of Powder Metallurgy, J. Mater. Process, Technol., Vol. 199, No. 1, 2008, pp. 417–424.

[6] Hewitt, R. L., Wallace, W., and De Malherbe, M. C., Plastic Deformation in Metal Powder Compaction, Powder Metall., Vol. 17, No. 33, 1974, pp. 1–12.

[7] Chtourou, H., Guillot, M., and Gakwaya, A., Modeling of the Metal Powder Compaction Process using the Cap Model, Part I. Experimental Material Characterization and Validation, Int. J. Solids Struct., Vol. 39, No. 4, 2002, pp. 1059–1075.

[8] Tahir, S. M., Ariffin, A. K., and Anuar, M. S., Finite Element Modelling of Crack Propagation in Metal Powder Compaction using Mohr-Coulomb and Elliptical Cap yield Criteria, Powder Technol., Vol. 202, No. 1–3, 2010, pp. 162–170.

[9] Schmidt, I., Trondl, A., Kraft, T., and Wonisch, A., Simulation of the Material Behaviour of Metal Powder During Compaction, Proc. Inst. Mech. Eng. Part E J. Process Mech. Eng., Vol. 224, No. 3, 2010, pp. 187–194.

[10] Zadeh, H. K., Jeswiet, J., and Kim, I. Y., Improvement in Robustness and Computational Efficiency of Material Models for Finite Element Analysis of Metal Powder Compaction and Experimental Validation, Int. J. Adv. Manuf. Technol., Vol. 68, No. 5–8, 2013, pp. 1785–1795.

[11] Babaei, H., Mostofi, T. M., Alitavoli, M., Namazi, N. and Rahmanpoor, A., Dynamic Compaction of Cold die Aluminum Powders, Geomech. Eng., Vol. 10, No. 1, 2016.

[12] Babaei, H., Mirzababaie Mostofi, T., Namdari-Khalilabad, M., Alitavoli, M., and Mohammadi, K., Gas Mixture Detonation Method, a Novel Processing Technique for Metal Powder Compaction: Experimental Investigation and Empirical Modeling, Powder Technol., Vol. 315, 2017, pp. 171–181.

[13] Nesterenko, V., Dynamics of Heterogeneous Materials, Springer Science & Business Media, 2013.

[14] Gourdin, W. H., Dynamic Consolidation of Metal

Powders, Prog. Mater. Sci., Vol. 30, No. 1, 1986, pp. 39–80.

[15] Trunin, R. F., Studies Performed in Russia into the Compressibility of Metals in Strong Shock Waves, High Temp., Vol. 42, No. 1, 2004, pp. 154–168.

[16] Babaei, H., Mostofi, T. M., and Sadraei, S. H., Effect of Gas Detonation on Response of Circular Plate-Experimental and Theoretical, Struct. Eng. Mech., Vol. 56, No. 4, 2015, pp. 535–548.

[17] Babaei, H., Mirzababaie Mostofi, T., Alitavoli, M., and Darvizeh, A., Empirical Modelling for Prediction of Large Deformation of Clamped Circular Plates in Gas Detonation Forming Process, Exp. Tech., Vol. 40, No. 6, 2016, pp. 1485–1494.

[18] Mostofi, T. M., Babaei, H., and Alitavoli, M., The Influence of Gas Mixture Detonation Loads on Large Plastic Deformation of thin Quadrangular Plates: Experimental Investigation and Empirical Modelling, Thin-Walled Struct., Vol. 118, 2017, pp. 1–11.

[19] Mostofi, T. M., Babaei, H., Alitavoli, M., Lu, G., and Ruan, D., Large Transverse Deformation of Double-Layered Rectangular Plates Subjected to Gas Mixture Detonation Load, Int. J. Impact Eng., Vol. 125, 2019, pp. 93–106.

[20] Mirzababaie Mostofi, T., Babaei, H., and Alitavoli, M., Experimental and Theoretical Study on Large Ductile Transverse Deformations of Rectangular Plates Subjected to Shock Load Due to Gas Mixture Detonation, Strain, Vol. 53, No. 4, 2017.

[21] Babaei, H., Mirzababaie Mostofi, T., and Alitavoli, M., Experimental Investigation and Analytical Modelling for Forming of Circular-Clamped Plates by using Gases Mixture Detonation, Proc. Inst. Mech. Eng. Part C J. Mech. Eng. Sci., 2015, pp. 095440621561433.

[22] Fahad, M. K., Stresses and Failure in the Diametral Compression Test, J. Mater. Sci., Vol. 31, No. 14, 1996, pp. 3723–3729.

[23] Babaei, H., Mostofi, T. M., and Alitavoli, M., Study on the Response of Circular thin Plate under Low Velocity Impact, Geomech. Eng., Vol. 9, No. 2, 2015.

[24] Babaei, H., Mirzababaie Mostofi, T., and Armoudli, E., On Dimensionless Numbers for the Dynamic Plastic Response of Quadrangular Mild Steel Plates Subjected to Localized and Uniform Impulsive Loading, Proc. Inst. Mech. Eng. Part E J. Process Mech. Eng., Vol. 231, No. 5, 2017, pp. 939–950.

[25] Babaei H., Mirzababaie Mostofi, T., New Dimensionless Numbers for Deformation of Circular Mild Steel Plates with Large Strains as a Result of Localized and Uniform Impulsive Loading, Proc. Inst. Mech. Eng. Part L J. Mater. Des. Appl., 2016, pp. 146442071665419.

[26] Mostofi, T. M., Babaei, H., Alitavoli, M., and Hosseinzadeh, S., On Dimensionless Numbers for Predicting Large Ductile Transverse Deformation of Monolithic and Multi-Layered Metallic Square Targets Struck Normally by Rigid Spherical Projectile, Thin-Walled Struct., Vol. 112, 2017, pp. 118–124.

[27] Mostofi, T. M., Babaei, H., and Alitavoli. M., Theoretical Analysis on the Effect of Uniform and Localized Impulsive Loading on the Dynamic Plastic Behaviour of Fully Clamped thin Quadrangular Plates, Thin-Walled Struct., Vol. 109, 2016, pp. 367-376.

[28] Rezasefat, M., Mostofi, T. M., and Ozbakkaloglu, T., Repeated Localized Impulsive Loading on Monolithic and Multi-Layered Metallic Plates, Thin-Walled Structures, Thin-Walled Struct., Vol. 144, 2019, pp. 106332,

[29] Rezasefat, M., Mirzababaie Mostofi, T., Babaei, H., Ziya-Shamami, M., and Alitavoli, M., Dynamic Plastic Response of Double-Layered Circular Metallic Plates due to Localized Impulsive Loading, Proc. Inst. Mech. Eng. Part L J. Mater. Des. Appl., Vol. 233, No. 7, 2019, pp. 1449-1471.